ADVANCED OPTICAL MATERIALS
www.advopticalmat.de

Giant Bulk Photostriction and Accurate Photomechanical Actuation in Hybrid Perovskites

Xingjie Lv, Shuai Dong, Xin Huang, Bo Cao, Shouxin Zeng, Yaojin Wang, Tom Wu, Lang Chen, Junling Wang, Guoliang Yuan, and Jun-Ming Liu*

It is well known that a material may be strained by mechanical, thermal, electric, magnetic, and light stimuli, and this effect has been extensively utilized in industries. However, the observed photostrictive effect usually occurs in the very thin surface layer and the photostriction of most bulk materials has been too small to be applied in a device until now. Here, a giant bulk photostriction is achieved, evidenced by the measured linear strain $\varepsilon \approx 0.72$–0.43% for $MAPbI_3$ single crystal plates of 0.05–0.5 mm in thickness under the 532 nm illumination. More importantly, the $MAPbI_3$ single crystals also exhibit accurate photomechanical actuation functionality and the actuator can precisely adjust the displacement from hundreds of pm to tens of μm or the angle of a hard mirror from $\approx 10^{-6}$ to 0.2 degree. The present work not only unveils the huge bulk photostriction in lead halide perovskite single crystals but also demonstrates a wireless photomechanical actuator which is much simpler and smaller than conventional piezoelectric actuators.

1. Introduction

Functionality of a material depends essentially on its composition and structure, manipulation of the crystal structure is one of the most important and straightforward approaches to generate and modify functionality. Crystal deformation, as driven by multiple stimuli such as temperature, pressure, strain, electric field/magnetic field, light, and so on,[1–4] represents one of the most popular functionalities already utilized for a number of practical applications. Substantial effort in further maximizing this functionality has been ongoing. For example, the piezoelectric effect, one of the most popular functionalities in our daily life and advanced technologies, deals with the inter-conversion between electric field and crystal strain.[1] Electrostriction effect, flexoelectric effect, and so on are also often utilized to generate strain.[2,3] Those excellent piezoelectric materials exhibit giant electro-controlled lattice strain and thus ultra-high precision as small as sub-nanometer in positioning can be realized by utilizing piezoelectric ceramics and single crystals. The best piezoelectric materials, such as $Pb(Mg_{1/3}Nb_{2/3})O_3$-$PbTiO_3$ (PMN-PT) single crystals, may achieve a bulk strain as large as 0.2–0.4% which can realize a number of high-precision positioning and sensing applications.[1]

In parallel to electro-control, another versatile approach, light-control can be also powerful for generating giant crystal strain through the so-called photostrictive effect.[4–11] Nevertheless, distinctly different from electro-control that may apply over the whole sample, light-control is more or less a surface effect since light illumination is usually absorbed within a thin surface layer in order to excite photocarriers. Therefore, photostriction is usually a surface effect rather than a bulk effect, noting that terminology "bulk strain" refers to the strain over a bulk sample. In other words, photostriction can be remarkable

X. Lv, B. Cao, S. Zeng, Y. Wang, G. Yuan
School of Materials Science and Engineering
Nanjing University of Science and Technology
Nanjing 210094, China
E-mail: yuanguoliang@njust.edu.cn

S. Dong
School of Physics
Southeast University
Nanjing 211189, China

X. Huang
New Energy Technology Engineering Laboratory of Jiangsu Province
Information Physics Research Center
School of Science
Nanjing University of Posts and Telecommunications
Nanjing 210023, China

T. Wu
School of Materials Science and Engineering
University of New South Wales (UNSW)
Sydney, NSW 2052, Australia

L. Chen, J. Wang
Department of Physics
Southern University of Science and Technology
Shenzhen 518055, China

J. Wang
Academy for Advanced Interdisciplinary Studies
Southern University of Science and Technology
Shenzhen 518055, China

J.-M. Liu
Laboratory of Solid State Microstructures
Nanjing University
Nanjing 210093, China

The ORCID identification number(s) for the author(s) of this article can be found under https://doi.org/10.1002/adom.202100837.

DOI: 10.1002/adom.202100837

in very thin samples but can't in bulk systems. For example, the bulk photostriction is only $\approx 6.4 \times 10^{-6}$ for bulk Si crystals and $\approx 7.8 \times 10^{-10}$ for bulk Ge crystals,[6,7] and they are too small to be utilizable for practical applications. On the other hand, for thin-film samples, photostriction can be large, as mentioned earlier. For example, Tsai reported a strain of $\approx 6.35 \times 10^{-3}$ in $MA_{0.25}FA_{0.7}Cs_{0.05}PbI_3$ films of thickness $d \approx 400$ nm.[12–14] This value is huge in comparison with the data on bulk Si and Ge crystals, but it is not a bulk strain.

Recently it was surprisingly reported that some bulk hybrid perovskites may exhibit large photostriction, and one case is the pioneering work of Zhou et al. reporting a photostriction as large as 5×10^{-5} in a 1.0 mm thick $MAPbI_3$ single crystal.[4] This result has stimulated substantial concern with possible giant bulk photostriction in these organo-lead halide perovskites (e.g., $MAPbX_3$ and its derivatives). It is noted that these solution-processed materials are excellent light absorption layers for remarkable photodetector,[15–18] superior solar cells with ≈25% power conversion efficiencies et al.[12,19–22]

It is natural to understand that the excellent photovoltaic performance is related to the super-long lifetime (τ_0), high mobility (μ), and long diffusion length (L_D) of the photocarriers.[23–25] Indeed, Shi et al. reported large $L_D > 10$ µm in $MAPbX_3$ (X = Br or I) single crystals[24] while Dong et al. found $L_D > 0.175$ mm in $MAPbI_3$ single crystals under 1 sun (100 mW cm^{-2}) illumination. Super large $L_D > 3$ mm under very weak illumination was found to be possible.[25] Given these lengths as far as a millimeter or more, it is a good start-point to ask whether these carriers can contribute to any lattice strain via photostrictive effect. This effect, if applicable, makes a giant bulk strain in these halide perovskites possible, thus adding an extraordinary functionality: giant bulk strain induced by light illumination.[5,6]

2. Results and Discussion

We perform a systematic investigation of this effect in bulk halide perovskites, and observe a giant bulk photostriction as large as 0.72–0.43% in the 0.05–0.5 mm thick $MAPbI_3$ single crystals. It is further suggested that the photocarriers with long diffusion length are responsible for this bulk strain: in association with the carrier transport, the special chemical bonds and dipoles in the MA organic groups are re-configured, triggering the giant bulk strain. Based on halide perovskites, we successfully fabricate a photomechanical actuator with pm-scale accuracy in addition to solar cells and luminescent devices.

Now we can check the possible bulk photostriction of $MAPbI_3$ single crystal. Here the atomic force microscopy (AFM) exhibits its high-resolution capability to detect the sample's displacement driven by the illumination, and a schematic drawing of the measuring geometry is plotted in **Figure 1**a. The crystal is 0.5 mm in thickness and the wavelengths (λ) of

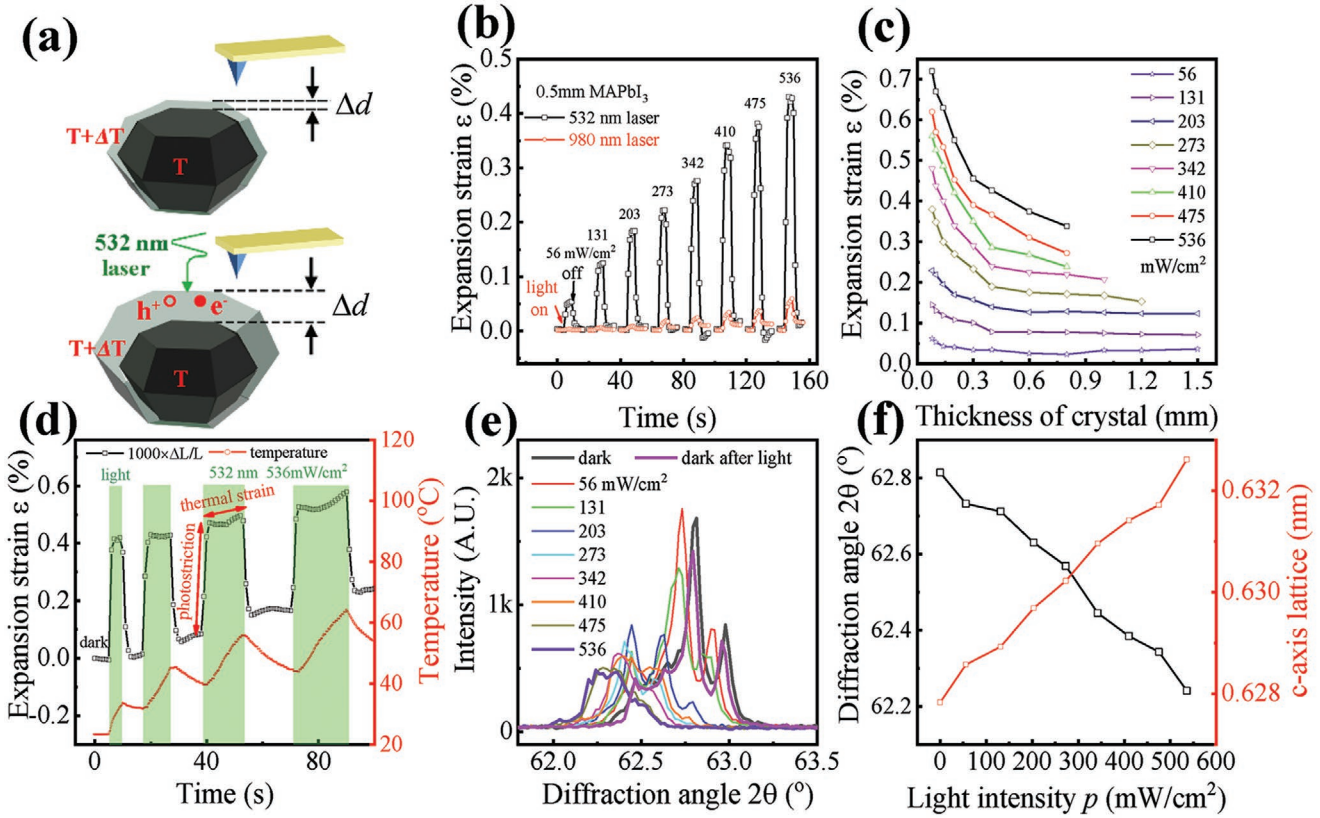

Figure 1. a) Sketch of pure thermal strain (top) and sketch of both photostriction and thermal strain (bottom), where T and ΔT are temperature and its change and h^+ and e^- are hole and electron. b) Expansion strain of the 0.5 mm thick crystal. c) Dependence of expansion strain on the thickness of crystal under 532 nm laser illumination. d) Dependencies of crystal expansion strain and temperature on time for the 0.5 mm thick crystal. e) XRD patterns of the $(330)_c$ crystal place and f) c-axis lattice of $MAPbI_3$ crystal in dark and under light illumination.

the two lasers are 532 and 980 nm respectively, noting that the 980 nm laser can pass through the crystal and likely heats the supporting stage.

It is surprising to find that the crystal under the 532 nm light illumination exhibits unexpected giant bulk strain (ε) though the incident lights are completely absorbed by the top surface layer. Here d is the crystal thickness along illumination direction, Δd is the thickness variation induced by light illumination, and ε is defined as $\Delta d/d$. The ε reaches up to 0.06% even if the laser's light intensity (p) is only 56 mW cm^{-2}, and it enhances up to 0.45% as p increases to 536 mW cm^{-2} (Figure 1b). Eventually, the sample's surface remains as good as the initial state in prior illumination, see Figure S1, Supporting Information. This 0.45% bulk strain is larger than those so far reported photostriction and is as good as the largest piezoelectric strains and magnetic shape memory strains reported so far, and. Regarding the dependence of bulk strain on the laser's p, the bulk strain ε increases linearly with increasing p, giving rise to an almost constant ratio $\varepsilon/p \approx 8.02 \times 10^{-7}$ m^2 W^{-1}.[4] Furthermore, the photostrictive efficiency ($\eta_{\text{eff}} = d\varepsilon/p$) also linearly increases with d increasing from $\approx 1 \times 10^{-10}$ w m^{-3} at $d = 0.08$ mm to $\approx 8 \times 10^{-10}$ w m^{-3} at $d = 1.5$ mm (Figure S2, Supporting Information).

A set of single crystals with different thicknesses were measured and their bulk strain ε-data are plotted in Figure 1c. The photostriction becomes larger as p is higher, and the 50 μm thick $MAPbI_3$ single crystal produces a $\varepsilon \approx 0.72\%$ when it is illuminated by the 532 nm laser with 536 mW cm^{-2}. However, the bulk strain falls down monotonously with increasing d.[26] This dependence is reasonable and consistent with the scenario that crystal expansion originates from the photocarriers with long L_D.[27–30] The photovoltaic short-circuit current (I_{sc}) and open-circuit voltage (V_{oc}) is ≈1.82 mA cm^{-2} and ≈1 V in the Au/$MAPbI_3$/Ga structure where the 532 nm lights with 170 mW cm^{-2} illuminate the semitransparent Au electrode of the 1 mm thick $MAPbI_3$ single crystal. This result suggests some photocarriers can diffuse across the 1 mm thick crystal and then contribute an I_{sc}.[25]

The bulk strain basically includes the large quick-response photostriction and the small slow-changing thermal strain.[31] To evidence this claim, a 0.5 mm thick crystal plate was illuminated by the 532 nm laser for different periods in the alternative turn-on/off sequence, while the crystal temperature was monitored using contacting thermocouples. Figure 1d shows the strain in response to the light-on/off for different periods (≈5–20 s). It is seen that an illumination for 5 s can heat the sample for 10 K in a slow and gradual mode. However, the bulk strain immediately reaches up to 0.4% after the light-on. The temperature response to the illumination is much slower than the bulk strain response. More interesting is that most crystal strain disappears immediately after the light-off while the sample's temperature does not. The ratio of thermal strain to total strain depends on the characteristic conditions and crystal quality and it is no more than 25% of the total strain in most cases (Figure S3, Supporting Information). In addition, as shown in Figure 1d, the long-time illumination for 10, 15, and 20 s would add some more features. Longer illumination leads to a higher sample's temperature and a longer time is needed for restoring the sample's temperature. The large photostriction shows a quick down-jump after the light-off. On the contrary, the crystal temperature cools down to room temperature and the relatively small thermal strain slowly decreases to zero within 90 s after the light-off. This experiment thus demonstrates that the photostriction response to light-on/off is sufficiently quick, while the thermal process and the associated lattice response are much slower.[31,32] Therefore, the observed crystal expansion shown in Figure 1b,c must be largely from the photostrictive effect.

The in situ XRD is employed to detect lattice expansion of the crystal surface layer. Figure 1e shows the XRD data of pseudo-cubic $(330)_c$ plane in the dark and then under light illumination. It is seen that the peak is located at $2\theta \approx 62.8°$ in the dark. During the illumination, this peak shifts towards the low-angle side, and the more the shift the higher the p, reaching $2\theta = 62.26°$ at $p = 536$ mW cm^{-2}. The c-axis lattice value is derived from the XRD pattern and it increases from 0.6278 to 0.6327 nm with p enhancing (Figure 1f). The strain of the surface layer is ≈ 0.78%, roughly consistent with the value of the 50 μm thick crystal measured by AFM tip.[12,14]

Furthermore, it is necessary to check the stability and accuracy of the bulk photostriction of the crystals. **Figure 2** shows the data of characterizations on a 0.5 mm thick $MAPbI_3$ crystal plate under the 532 nm illumination in various modes. First, the top surface displacements Δd in response to the cycled light-on/off sequence at different p ≈ 56–536 mW cm^{-2}, are plotted in Figure 2a. Since the thermal strain changes slowly, the cycle with 5 s in light and 5 s in dark was applied to decrease the fluctuation of thermal strain. The crystal demonstrates the excellent linear strain in response to p without any hysteresis, and the maximal displacement reaches up to 2.0 μm (Figure 2b). Second, Figure 2c shows the cycling stability of the strain switching upon the light-on/off cycles at $p = 273$ mW cm^{-2}. While a slight reduction of Δd in the first 100 cycles is seen, the subsequent 2000-cycling test shows a high repeatability of strain switching. Furthermore, the displacement with pm-scale accuracy is introduced in a $MAPbI_3$ single crystal as shown in Figure 2d. The ≈400 pm displacement is introduced by the light of a commercial LED lamp with the price of 0.5 USD dollars (Figure S4, Supporting Information). The light with different p can easily be achieved by changing the distance (R) between the LED lamp and the single crystal according to the relationship of $p \propto R^{-2}$. The slight fluctuation of displacement mainly comes from the instability of LED light source. For comparison, the periodic displacement is not observed in the PZT ceramic under an intermittent light illumination.

The generation of bulk strain in $MAPbI_3$ crystals may involve two processes. In the first process, photon absorption excites a mass of electron-hole pairs in the thin surface layer under illumination, and subsequently the charges transfer from hybridized Pb 6s–I 5p orbitals to the Pb 6p orbitals (Figure S5, Supporting Information).[4,33–35] The surface layer is very thin since the lights with 400–800 nm wavelength just have the penetration depth of ≈100 nm (Figure S6, Supporting Information). This process expands the Pb—I—Pb bond and enlarges the interatomic spacing leading to the crystal expansion. In the second process, the generated free electrons and holes diffuse into the crystal interior. The separation of electrons and holes would induce a diffusion potential and a built-in electric field. The dipolar MA cations can align along the built-in field in a local region[36,37]

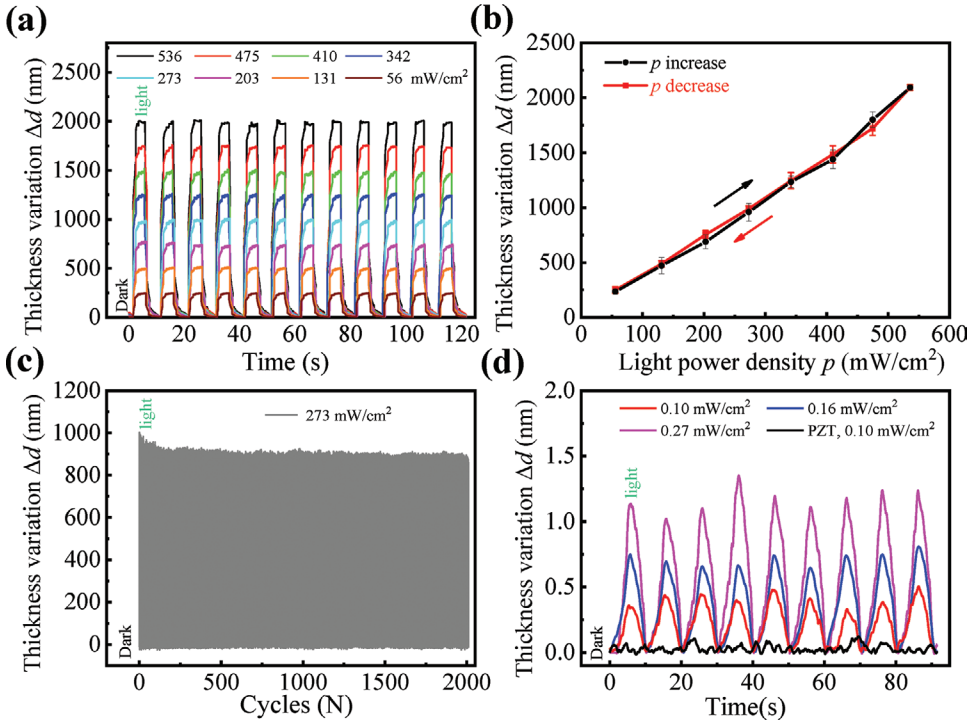

Figure 2. a) Initial cycles of thickness variation Δd of a 0.5 mm thick $MAPbI_3$ crystal periodically triggered by 532 nm light illumination. b) Linearity of Δd versus light power density p curves. c) 2000 light-dark cycles of Δd periodically triggered by lights with 273 mW cm^{-2}. d) Precise Δd with pm-scale accuracy for the crystal periodically under weak light illumination.

and the MA reorientation induces a large amplitude of structural motions and lattice distortions via the strong coupling of the translation-rotation and acoustic phonons.[38–40] In principle, the injected carriers by bias can introduce a crystal strain like photocarriers. The calculated photocarriers density at the crystal surface is about $\approx 10^{19}$ s^{-1} m^{-2} when the $MAPbI_3$ single crystal is illuminated by the 532 nm lights with 56 mW cm^{-2}. Meanwhile, the injected carrier density is $\approx 10^{13}$ s^{-1} m^{-2} when the dark $MAPbI_3$ single crystal is under 45 V bias (Figure S7, Supporting Information). The density of photocarriers is $\approx 10^6$ more than that of injected carriers, so the photostriction is far stronger than the electrostriction introduced by injected carriers. Besides, it should be mentioned that the photovoltaic voltage (<1.5 V) may contribute a very weak bulk strain via, for example, electrostriction or inverse piezoelectric mechanism.

Given the giant bulk strain observed in the $MAPbI_3$ crystals, it is essential to discuss the possible scenario in which how the long-distance drifting photocarriers can generate large photostriction. It is believed that MA organic structure in the tetragonal $MAPbI_3$ crystals exhibits an order-disorder phase transition which introduces a nonzero but small electric polarization, leading to the formation of polar nanodomains.[41–46] These local polarized regions would be very helpful for suppressing the carrier scattering. Similar scenarios were once proposed by Zhu et al., and it was believed that the screened Coulomb potential created by large polarons in the crystal can reduce the carrier scattering by charged defects and phonons.[23,47,48] This is the so-called large polaron model that provides a platform to explain why hybrid perovskite-based defect-tolerant semiconductors have super-long τ_0 and L_D. To understand the observed effects, the ab initio calculation was done based on density functional theory (DFT).[49–52] Since the photon-induced expansion is a macroscopic effect, our calculations focus on charge neutrality. At room temperature, the structure of $MAPbI_3$ is tetragonal, whose unit cell contains four polar MA molecular groups, located at the center of four lead iodide cages. Each MA molecule is polar, with both polarization components along the *c*-axis and in the *ab* plane. There are different possible orientations of MA molecules, leading to polar and nonpolar orientations. Considering the symmetry, four most possible configurations corresponding to the four MA orientations are taken into consideration and the optimized structure constants and energies are shown in **Table 1**. It is clear that the

Table 1. The optimized lattice constants, volumes, and calculated total energies for $CH_3NH_3PbI_3$ in different configurations of the MA orientations. The blue balls represent the four MA molecular groups in the unit cell, which are labeled as 1, 2, 3, and 4. The orientations of corresponding MA molecules are denoted by the blue arrows.

Formula	Configurations of MA dipoles	Lattice constants [Å]	Volume [$Å^3$ $f.u.^{-1}$]	Energy [meV $f.u.^{-1}$]
$CH_3NH_3PbI_3$		$a = 9.086$, $b = 9.106$, $c = 12.853$	265.83	24
		$a = 9.025$, $b = 9.164$, $c = 12.704$	262.29	0
		$a = 9.123$, $b = 9.068$, $c = 12.717$	262.85	19
		$a = 9.091$, $b = 9.067$, $c = 12.823$	264.15	0.3

one with the lowest energy is non-polar, with all dipole components canceled out. However, those polar ones with uncompensated components are only slightly higher in energy but also slightly larger in volume. For example, in the fully polar limit with all dipoles align parallelly, the volume is 1.35% larger than the lowest energy one. Thus, the built-in field from light-generated photocarriers can partially polarize the MA molecules, which increases the ratio of polar MA configurations over the whole crystal and thus leads to the slight expansion of $MAPbI_3$ crystal.[39,53] However the simulated volume expansion due to MA molecular groups just contributes the photostriction of 0.45% which is smaller than the maximum strain measured by XRD (≈0.76%) and AFM (≈0.72%). Therefore, there are other factors for the photostriction of halide perovskite semiconductors with long L_D. In fact, the photocarriers can introduce an obvious photostriction in the $CsPbBr_3$ single-crystal though its value is much smaller than that of $MAPbI_3$ with the same characteristic conditions.[43]

Given the giant bulk photostriction of the $MAPbI_3$ single crystals, we can demonstrate a prototype actuation device that can be light-driven and thus controlled remotely. The strain near the photon-absorbing region would be greater and thus the local lattice expansion becomes more remarkable. This feature of non-uniform deformation in the crystal should be concerned if an advice is designed for specific functionality.

These excellent properties of the as-prepared crystals allow us to fabricate a remotely controlled photomechanical actuator, and one demonstration is shown in **Figure 3**a where the path of a light beam is precisely manipulated by the actuator fabricated in the present work. A $3.4 \times 3.4 \times 3.4$ mm^3 $MAPbI_3$ single crystal is used, and the 532 nm laser illumination for actuation is aligned onto the left side surface. The crystal deformation in this geometry depends on the inhomogeneous strain distribution across the crystal, and the left and right side surfaces exhibit the largest and smallest transverse expansions, respectively. Once the bottom plane of the crystal is fixed, the top plane will be inclined at an angle, that is, $\Delta\theta$. A rigid mirror with 0.2 mm in thickness is attached to the top plane. Thus, the signal light reflected by the mirror would rotate for $2\Delta\theta$ in response to the crystal top-surface inclination. The measured data support

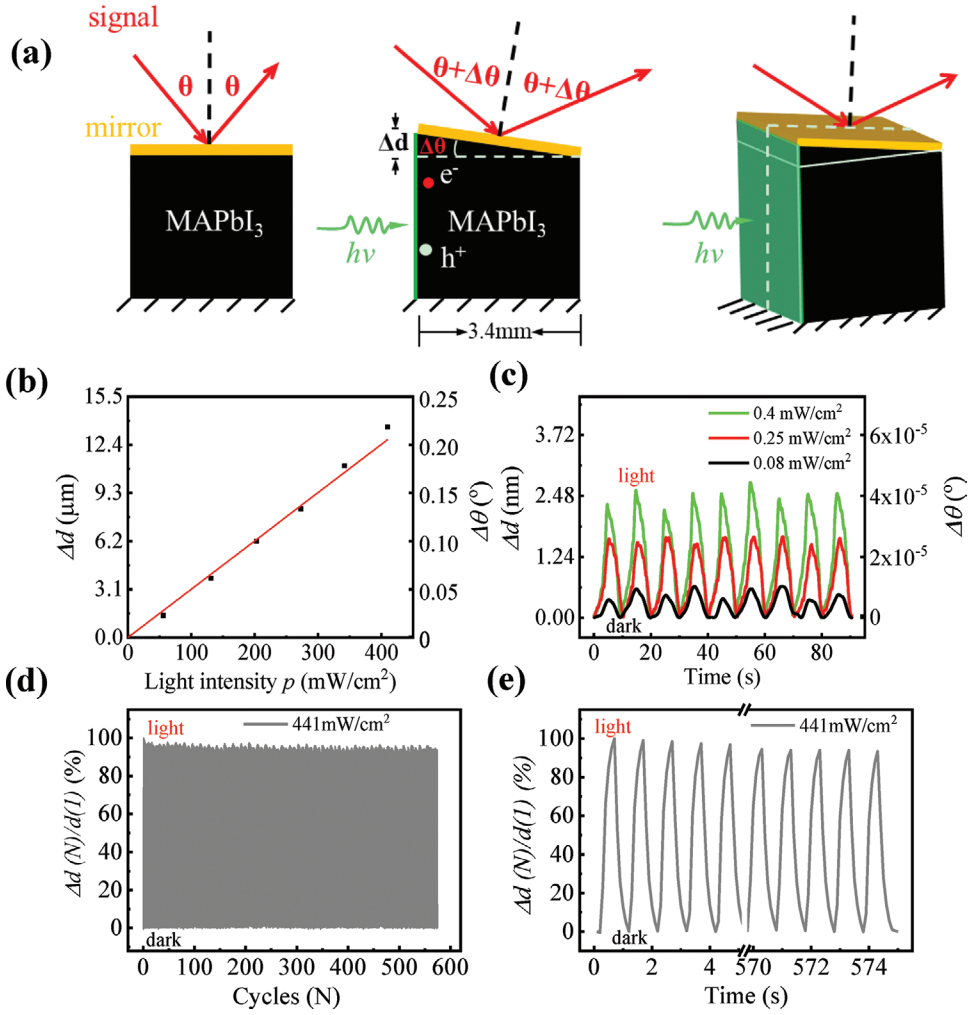

Figure 3. a) Sketch on the photomechanical actuation for precision light path control, where θ is the incident angle of signal laser and $\Delta\theta$ is the angle difference due to the crystal expansion. b) Dependence of Δd and $\Delta\theta$ on light intensity p. c) Dependence of the tiny Δd and $\Delta\theta$ values on time to estimate accuracy. d,e) Dependence of $\Delta d(N)/\Delta d(1)$ on the dark/light cycles (N).

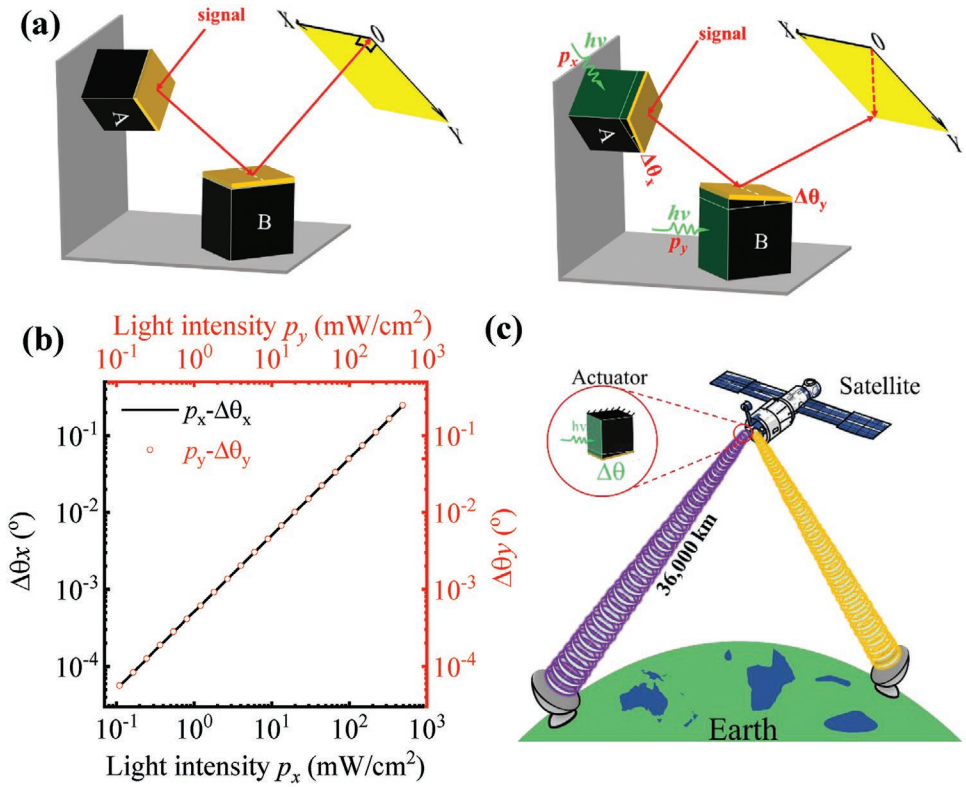

Figure 4. a) Sketch on two actuators controlling a laser spot in the *X*-*Y* plane. b) Signal light's angle manipulation (i.e. $\Delta\theta_x$ and $\Delta\theta_y$) through adjusting p_x and p_y, where $\Delta X = L\sin(2\Delta\theta_x)$, $\Delta Y = L\sin(2\Delta\theta_y)$, and L is the optical distance between the actuators and the *X*-*Y* plane. c) Precise signal light control between satellite and earth for quantum communications.

the approximately linear relationships: $\Delta\theta$ (°) ≈ 5.03×10^{-4} p, Δd (μm) ≈ 0.0311 p, and ε (%) ≈ 0.00092 p (Figure 3b). Under a very weak light intensity such as $p \approx 0.016$ mW cm^{-2}, Δd is as small as 500 pm and $\Delta\theta$ is about 8×10^{-6} degrees (Figure 3c) which are good enough to precisely control the super long light path with thousands of kilometers for quantum communications. Besides, such wireless and small $MAPbI_3$-based actuators are certainly highly favored for miniaturized optical device applications. Furthermore, the stability and repeatability of the light-driven actuator are verified by the dependence of the normalized Δd (i.e., $\Delta d(N)/\Delta d(1)$) on the light/dark cycles number (N) in Figure 3d. In fact, the $\Delta d(574)/\Delta d(1)$ is over 94% in Figure 3e.

As shown in **Figure 4**a, the A and B actuators with certain angles are located on the two planes perpendicular to each other so that they can drive the signal light move ΔX and ΔY in another plane perpendicular to the origin signal light, respectively. That is to say, the p of 532 nm light upon the A and B actuators (i.e., p_x and p_y) control ΔX and ΔY independently (Figure 4b). Since either Δd or $\Delta\theta$ is approximately linearly proportional to the small p of the 532 nm light, this two-actuator combination can control super long light path conventionally. For example, if the actuator in an artificial satellite has a tiny $\Delta\theta$ of ≈8×10^{-6} degrees to manipulate the signal light, its light spot will move ≈10 m on earth (Figure 4c).

Now we show you several advantages of the $MAPbI_3$-based actuator over the state-of-merit PZT-based actuators.[1,55,56] First, the $MAPbI_3$-based actuator can be remotely driven by 532 nm light from a commercial LED lamp or a laser. Second, such a wireless actuator is much smaller and lighter than the PZT-based actuators (integrated power source is needed). It is known that a PZT ceramic actuator commonly shows a ≈0.1–0.3% strain driven by an electric field as high as 20 kV cm^{-1}, which implies that a 3.0 mm thick PZT ceramic plate may be elongated for ≈3–9 μm with a driving voltage over 6 kV.[1,54] Currently, the multilayer actuator composed of thousands of ≈50 μm thick piezoelectric slices and inner electrodes is developed, but the driving voltage of about ≈100 V still requires a heavy external power source. Third, the as-grown $MAPbI_3$ single crystals are usually millimeters in size, and they are light-driven actuators with pm-scale accuracy. Therefore, the actuator fabrication is simple and cost-effective in comparison with the complex structure and high cost of the multilayer PZT-based actuator.[1,55] Fourth, the light-driven actuator shows greater strain than those PZT-based actuators. Fifth, the crystal strain shows an excellent linear relationship with the laser intensity p, while commercial piezoelectric actuators usually exhibit nonzero hysteresis which is not favorable. Therefore, a $MAPbI_3$-based photomechanical actuator is promising to be used in many scenes where the piezoelectric actuator and its power source are too large and too heavy to be applied.[56]

In view of the challenges of instability and Pb contamination of halide perovskite thin films in meter-scale solar cells, it is urgent to develop high value-added and tiny devices such as chips and actuators with a single crystal. The mm thick $MAPbI_3$ single crystal is much more stable than the μm-thick $MAPbI_3$ film, and the mm-scale actuator needs less Pb content

than that of the meter-scale solar cells, so photomechanical actuator will be one of the most important applications of lead halide perovskite semiconductor.

3. Conclusion

In conclusion, the 0.05–0.5 mm thick $MAPbI_3$ crystals show a 0.72–0.43% photostriction due to the photocarriers excited by the 532 nm laser with 536 mW cm^{-2}. At first, the laser excites photocarriers, which lengthens some chemical bonds and induces a crystal expansion at the surface layer of the crystal. Then the excess photocarriers diffuse into the interior of the $MAPbI_3$ crystal, reorient dipoles, and finally introduce a giant bulk photostriction in a mm thick crystal. Most important, the $MAPbI_3$ single crystal can act as a photomechanical actuator with pm-scale accuracy. Compared with the piezoelectric actuator, this novel actuator has many merits such as wireless, light, small, simple structure, cost-effective, giant strain, and linear relationship between crystal strain and laser intensity. This study not only proves that the photocarriers can introduce a giant bulk photostriction in the mm-scale thick $MAPbI_3$ crystal but also add new freedom to develop novelty photomechanical and photoelectronic devices with halide perovskite.

4. Experimental Section

Growth of $MAPbI_3$ Single Crystals and Structure Characterization: High purity PbI_2 (99.99%, Aladdin) powders, MAI (MA = $CH_3NH_3^+$, Advanced Election Technology Co.,Ltd) powders, and γ-Butyrolactone (GBL, ≥99.9%, Aladdin) liquid were used to prepare the $MAPbI_3$ single crystal.[4] At first, PbI_2 and MAI were dissolved in GBL solvent to prepare 1 mol L^{-1} solution. The iodide solution was heated up to 60 °C, and then these solutions were mixed and stirred to prepare $MAPbI_3$ solution. Insoluble substances and impurities in the mother solution were removed with the filter paper with 0.2 µm pore size. After that, the 2 mL $MAPbI_3$ solution was gradually heated to ≈95 °C to grow seed crystals in a small bottle. A high-quality seed crystal was chosen and placed in the $MAPbI_3$ saturated solution to grow a large-size crystal within 3–6 h. Furthermore, XRD (Bruker D8 Advanced) patterns were used to measure these crystals in light or in dark.[12]

Simulation of Crystal Expansion: The DFT calculations were performed using Vienna ab initio simulation package (VASP).[49] The generalized gradient approximation (GGA) functional of Perdew, Burke, and Ernzerhof (PBE) was used as exchange-correlation potentials.[50–52] The plane-wave cutoff energy was 500 eV. The self-consistent energy convergence accuracy was set as follows: 1×10^{-5} eV for structural relaxations and 1×10^{-6} eV for static calculations. All structures were fully relaxed by using the conjugate gradient method until the Hellmann–Feynman forces acting on each atom were less than 0.02 eV $Å^{-1}$. Automatically generated Γ-centered *k*-point grid of $6 \times 6 \times 4$ was used for $MAPbI_3$.

Photostriction and Photomechanical Actuators: The commercial AFM (Bruker multimode 8) was used to characterize the surface and the crystal expansion in light.[4] The laser beams with 532 and 980 nm wavelength (λ) and 1 cm^2 light spot were chosen to characterize crystal expansion in light. The light power density *p* at the sample location was carefully calibrated using a commercial energy meter (Newport, 91,150V). Furthermore, AFM tip (Bruker SCANASYST-AIR, 2 nm radius) scanned a fixed location to get 128×128 thickness data one by one during the light periodically irradiating on the surface within 122 s, and the thickness profile as a function of time was acquired. $MAPbI_3$, Fe, $SrTiO_3$, quarts, and glass were characterized in the same way to access system errors. Furthermore, the photomechanical actuators were prepared with the three processes. At first, a $3.4 \times 3.4 \times 0.2$ mm^3 mirror was fixed on the top surface of each $MAPbI_3$ crystal with a $3.4 \times 3.4 \times 3.4$ mm^3 shape, and then two of these $MAPbI_3$ single crystals (i.e., A and B actuators) were placed on the two orthogonal planes of a holder, respectively. Second, through changing the position and angle of the signal laser and crystals, the mirrors reflected the signal red light with 650 nm wavelength and the projection of such light on the top surface of the crystal was perpendicular to the side surface of the crystal where the other laser with 532 nm wavelength vertical illuminated for crystal expansion and inclining mirror. Third, each laser with 532 nm wavelength induced the crystal expansion of its actuators and drives the signal light to move ΔX and ΔY in the *X*-*Y* plane that was vertical to the original signal light.

Supporting Information

Supporting Information is available from the Wiley Online Library or from the author.

Acknowledgements

X.L., S.D., and X.H. contributed equally to this work. The National Natural Science Foundation of China (51790492, 51721001, 11834002, and 61874055) and the National Key Research Program of China (2016YFA0300101) supported the works.

Conflict of Interest

The authors declare no conflict of interest.

Data Availability Statement

Research data are not shared.

Keywords

bulk photostriction, halide perovskites, $MAPbI_3$, photomechanical actuators

Received: April 26, 2021
Revised: July 14, 2021
Published online: August 3, 2021

[1] E. W. Sun, W. W. Cao, *Prog. Mater. Sci.* **2014**, *65*, 124.
[2] B. Chen, T. Li, Q. F. Dong, E. Mosconi, J. F. Song, Z. L. Chen, Y. H. Deng, Y. Liu, S. Ducharme, A. Gruverman, F. D. Angelis, J. S. Huang, *Nat. Mater.* **2018**, *17*, 1020.
[3] L. L. Shu, S. M. Ke, L. F. Fei, W. B. Huang, Z. G. Wang, J. H. Gong, X. N. Jiang, L. Wang, F. Li, S. J. Lei, Z. G. Rao, Y. B. Zhou, R.-K. Zheng, X. Yao, Y. Wang, M. Stengel, G. Catalan, *Nat. Mater.* **2020**, *19*, 605.
[4] Y. Zhou, L. You, S. W. Wang, Z. L. Ku, H. J. Fan, D. Schmidt, A. Rusydi, L. Chang, L. Wang, P. Ren, L. F. Chen, G. L. Yuan, L. Chen, J. L. Wang, *Nat. Commun.* **2016**, *7*, 11193.
[5] T.-C. Wei, H.-P. Wang, T.-Y. Li, C.-H. Lin, Y.-H. Hsieh, Y.-H. Chu, J.-H. He, *Adv. Mater.* **2017**, *29*, 1701789.
[6] B. Kundys, *Appl. Phys. Rev.* **2015**, *2*, 011301.

[7] J. R. Buschert, R. Colella, *Solid State Commun.* **1991**, *80*, 419.
[8] T. J. White, *Photomechanical Materials, Composites, and Systems: Wireless Transduction of Light Into Work*, Wiley, Hoboken, NJ **2017**.
[9] X. N. Dong, F. Tong, K. M. Hanson, R. O. Al-Kaysi, D. Kitagawa, S. Kobatake, C. J. Bardeen, *Chem. Mater.* **2019**, *31*, 1016.
[10] P. Naumov, S. Chizhik, M. K. Panda, N. K. Nath, E. Boldyreva, *Chem. Rev.* **2015**, *115*, 12440.
[11] X. N. Dong, T. Y. Guo, D. Kitagawa, S. Kobatake, P. Palffy-Muhoray, C. J. Bardeen, *Adv. Funct. Mater.* **2020**, *30*, 1902396.
[12] H. Tsai, R. Asadpour, J.-C. Blancon, C. C. Stoumpos, O. Durand, J. W. Strzalka, B. Chen, R. Verduzco, P. M. Ajayan, S. Tretiak, J. Even, M. A. Alam, M. G. Kanatzidis, W. Y. Nie, A. D. Mohite, *Science* **2018**, *360*, 67.
[13] N. Rolston, R. B. Kennett, L. T. Schelhas, J. M. Luther, J. A. Christians, J. J. Berry, R. H. Dauskardt, *Science* **2020**, *368*, eaay8691.
[14] H. Tsai, W. Y. Nie, A. D. Mohite, *Science* **2020**, *368*, eaba6295.
[15] C.-H. Lin, B. Cheng, T.-Y. Li, J. R. D. Retamal, T.-C. Wei, H.-C. Fu, X. S. Fang, J.-H. He, *ACS Nano* **2019**, *13*, 1168.
[16] W. Yang, J. X. Chen, Y. Zhang, Y. J. Zhang, J.-H. He, X. S. Fang, *Adv. Funct. Mater.* **2019**, *29*, 1808182.
[17] H.-P. Wang, S. Y. Li, X. Y. Liu, Z. F. Shi, X. S. Fang, J.-H. He, *Adv. Mater.* **2021**, *33*, 2003309.
[18] X. W. Guan, X. C. Yu, D. Periyanagounder, M. R. Benzigar, J.-K. Huang, C.-H. Lin, J. Y. Kim, S. Singh, L. Hu, G. Z. Liu, D. H. Li, J.-H. He, F. Yan, Q. J. Wang, T. Wu, *Adv. Opt. Mater.* **2021**, *9*, 2001708.
[19] Best research-cell efficiency chart, www.nrel.gov/pv/cell-efficiency.html (accessed: May 2021).
[20] W.-W. Liu, T.-H. Wu, M.-C. Liu, W.-J. Niu, Y.-L. Chueh, *Adv. Mater. Interfaces* **2019**, *6*, 1801758.
[21] C.-H. Lin, C.-Y. Kang, T.-Z. Wu, C.-L. Tsai, C.-W. Sher, X. W. Guan, P.-T. Lee, T. Wu, C.-H. Ho, H.-C. Kuo, J.-H. He, *Adv. Funct. Mater.* **2020**, *30*, 1909275.
[22] Z. J. Liu, C.-H. Lin, B.-R. Hyun, C.-W. Sher, Z. J. Lv, B. Q. Luo, F. L. Jiang, T. Wu, C.-H. Ho, H.-C. Kuo, J.-H. He, *Light: Sci. Appl.* **2020**, *9*, 83.
[23] K. Miyata, X.-Y. Zhu, *Nat. Mater.* **2018**, *17*, 379.
[24] D. Shi, V. Adinolfi, R. Comin, M. J. Yuan, E. Alarousu, A. Buin, Y. Chen, S. Hoogland, A. Rothenberger, K. Katsiev, Y. Losovyj, X. Zhang, P. A. Dowben, O. F. Mohammed, E. H. Sargent, O. M. Bakr, *Science* **2015**, *347*, 519.
[25] Q. F. Dong, Y. J. Fang, Y. C. Shao, P. Mulligan, J. Qiu, L. Cao, J. S. Huang, *Science* **2015**, *347*, 967.
[26] D. Kim, J. S. Yun, P. Sharma, D. S. Lee, J. Kim, A. M. Soufiani, S. J. Huang, M. A. Green, A. W. Y. Ho-Baillie, J. Sedel, *Nat. Commun.* **2019**, *10*, 444.
[27] C. Wehrenfennig, G. E. Eperon, M. B. Johnston, H. J. Snaith, L. M. Herz, *Adv. Mater.* **2014**, *26*, 1584.
[28] A. K. Jena, A. Kulkarni, T. Miyasaka, *Chem. Rev.* **2019**, *119*, 3036.
[29] L. M. Pazos-Outón, M. Szumilo, R. Lamboll, J. M. Richter, M. Crespo-Quesada, M. Abdi-Jalebi, H. J. Beeson, M. Vrućinić, M. Alsari, H. J. Snaith, B. Ehrler, R. H. Friend, F. Deschler, *Science* **2016**, *351*,1430.
[30] J. S. Huang, Y. B. Yuan, Y. C. Shao, Y. F. Yan, *Nat. Rev. Mater.* **2017**, *2*, 17042.
[31] M. Keshavarz, M. Ottesen, S. Wiedmann, M. Wharmby, R. Küchler, H. Yuan, E. Debroye, J. A. Steele, J. Martens, N. E. Hussey, M. Bremholm, M. B. J. Roeffaers, J. Hofkens, *Adv. Mater.* **2019**, *31*, 1900521.
[32] C. Y. Ge, M. Y. Hu, P. Wu, Q. Tan, Z. Z. Chen, Y. P. Wang, J. Shi, J. Feng, *J. Phys. Chem. C* **2018**, *122*, 15973.
[33] X.-Y. Zhu, V. Podzorov, *J. Phys. Chem. Lett.* **2015**, *6*, 4758.
[34] K. Miyata, D. Meggiolaro, M. T. Trinh, P. P. Joshi, E. Mosconi, S. C. Jones, F. D. Angelis, X.-Y. Zhu, *Sci. Adv.* **2017**, *3*, e1701217.
[35] V. D'Innocenzo, G. Grancini, M. J. P. Alcocer, A. R. S. Kandada, S. D. Stranks, M. M. Lee, G. Lanzani, H. J. Snaith, A. Petrozza, *Nat. Commun.* **2014**, *5*, 3586.
[36] M. Saba, M. Cadelano, D. Marongiu, F. P. Chen, V. Sarritzu, N. Sestu, C. Figus, M. Aresti, R. Piras, A. G. Lehmann, C. Cannas, A. Musinu, F. Quochi, A. Mura, G. Bongiovanni, *Nat. Commun.* **2014**, *5*, 5049.
[37] A. Miyata, A. Mitioglu, P. Plochocka, O. Portugall, J. T.-W. Wang, S. D. Stranks, H. J. Snaith, R. J. Nicholas, *Nat. Phys.* **2015**, *11*, 582.
[38] R. E. Wasylishen, O. Knop, J. B. Macdonald, *Solid State Commun.* **1985**, *56*, 581.
[39] A. Poglitsch, D. Weber, *J. Chem. Phys.* **1987**, *87*, 6373.
[40] A. M. A. Leguy, J. M. Frost, A. P. McMahon, V. G. Sakai, W. Kockelmann, C. H. Law, X. E. Li, F. Foglia, A. Walsh, B. C. O'Regan, J. Nelson, J. T. Cabral, P. R. F. Barnes, *Nat. Commun.* **2015**, *6*, 7124.
[41] M. A. Qaiser, X. Z. Ma, R. T. Ma, W. Ali, X. J. Xu, G. L. Yuan, L. Chen, *J. Am. Ceram. Soc.* **2019**, *102*, 5424.
[42] J. J. Li, X. Zhou, Z. F. Liu, *Adv. Opt. Mater.* **2020**, *8*, 2000886.
[43] J. Xue, D. D. Yang, B. Cai, X. B. Xu, J. Wang, H. Ma, X. C. Yu, G. L. Yuan, Y. S. Zou, J. Z. Song, H. B. Zeng, *Adv. Funct. Mater.* **2019**, *29*, 1807922.
[44] L. M. Garten, D. T. Moore, S. U. Nanayakkara, S. Dwaraknath, P. Schulz, J. Wands, A. Rockett, B. Newell, K. A. Persson, S. T. McKinstry, D. S. Ginley, *Sci. Adv.* **2019**, *5*, eaas9311.
[45] H. Röhm, T. Leonhard, A. D. Schulz, S. Wagner, M. J. Hoffmann, A. Colsmann, *Adv. Mater.* **2019**, *31*, 1806661.
[46] Y.-J. Kim, T.-V. Dang, H.-J. Choi, B.-J. Park, J.-H. Eom, H.-A. Song, D. Seol, Y. Kim, S.-H. Shin, J. Nah, S.-G. Yoon, *J. Mater. Chem. A* **2016**, *4*, 756.
[47] K. Xu, X. Z. Lu, H. J. Xiang, *npj Quantum Mater.* **2017**, *2*, 1.
[48] B. Y. Huang, G. L. Kong, E. N. Esfahani, S. L. Chen, Q. Li, J. X. Yu, N. A. Xu, Y. Zhang, S. H. Xie, H. D. Wen, P. Gao, J. J. Zhao, J. Y. Li, *npj Quantum Mater.* **2018**, *3*, 30.
[49] A. Létoublon, S. Paofai, B. Rufflé, P. Bourges, B. Hehlen, T. Michel, C. Ecolivet, O. Durand, S. Cordier, C. Katan, J. Even, *J. Phys. Chem. Lett.* **2016**, *7*, 3776.
[50] R. M. Lynden-Bell, K. H. Michel, *Rev. Mod. Phys.* **1994**, *66*, 721.
[51] G. Kresse, J. Furthmüller, *Phys. Rev. B* **1996**, *54*, 11169.
[52] G. Kresse, D. Joubert, *Phys. Rev. B* **1999**, *59*, 1758.
[53] J. M. Frost, K. T. Butler, F. Brivio, C. H. Hendon, M. V. Schilfgaarde, A. Walsh, *Nano Lett.* **2014**, *14*, 2584.
[54] Z. R. Gao, X. F. Sun, Y. Y. Wu, Y. Z. Wu, H. L. Cai, X. S. Wu, *J. Phys. Chem. Lett.* **2019**, *10*, 2522.
[55] J. Even, M. Carignano, C. Katan, *Nanoscale* **2016**, *8*, 6222.
[56] J. P. Perdew, K. Burke, M. Ernzerhof, *Phys. Rev. Lett.* **1996**, *77*, 3865.